Supporting Information for

Tuning Valley-Ohmic Contact and Interfacial Electronic Properties in Valley-Polarized Semiconductor/Dirac Semimetal Heterostructures

Hao Guo,[ab] Yongqian Zhu,[ac] Jinbo Pan,*[ac] Shixuan Du[acd]

[a] *Beijing National Laboratory for Condensed Matter Physics, Institute of Physics, Chinese Academy of Sciences, Beijing 100190. E-mail: jbpan@iphy.ac.cn*

[b] *School of Urban Construction, Hebei Normal University of Science & Technology, Qinhuangdao 066004, China.*

[c] *School of Physics, University of Chinese Academy of Sciences, Beijing 100049, China.*

[d] *Songshan Lake Materials Laboratory, Dongguan 523808 Guangdong, China.*

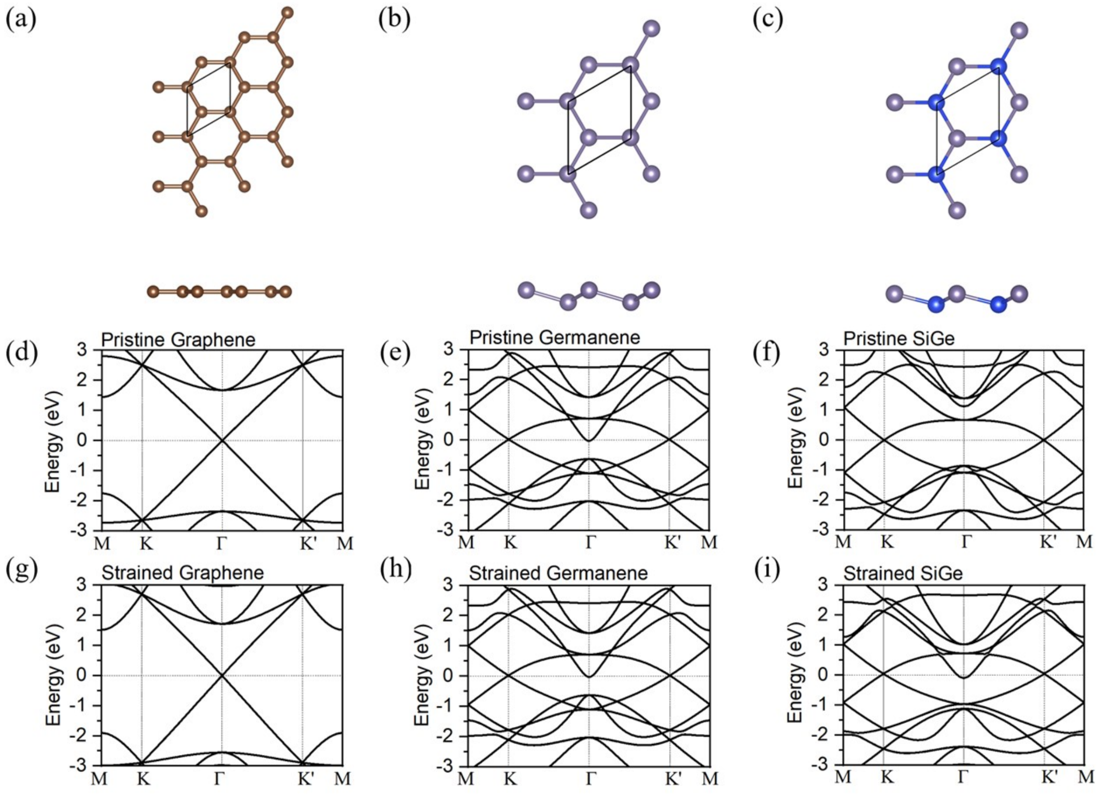

Fig. S1. The lattice structures and band structures of the Dirac semimetals *X*. The top and side views of (a) graphene, (b) germanene, and (c) SiGe, respectively. The pristine and strained band structures of (d,g) graphene, (e,h) germanene, and (f,i) SiGe, respectively. The Fermi level is set to 0 eV.

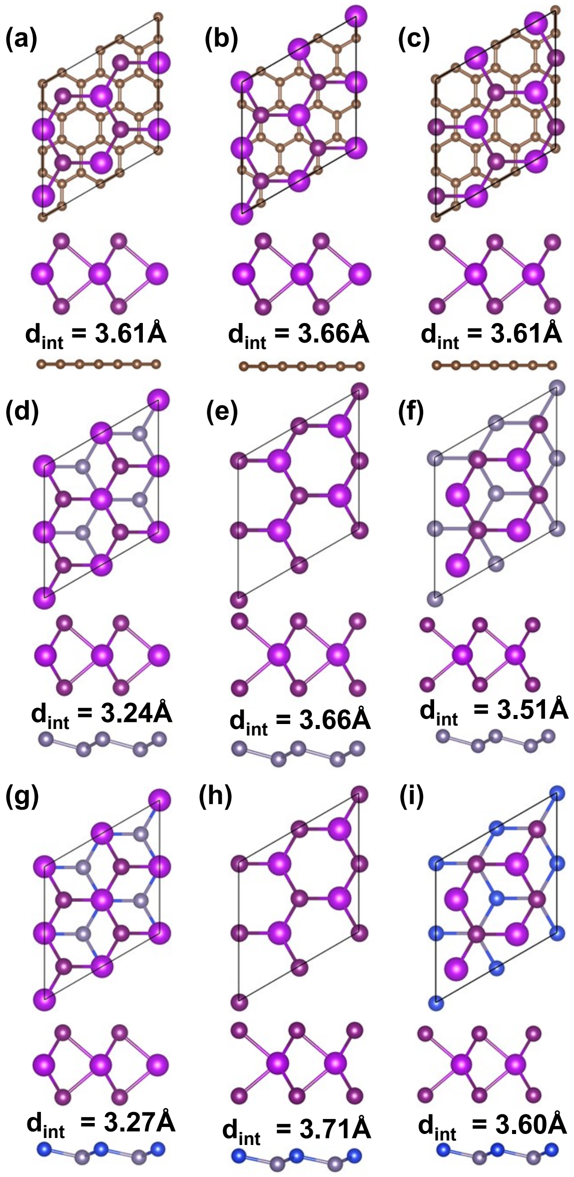

Fig. S2. Different stacking patterns of *X*/GdI$_2$ (*X* = graphene, germanene, and SiGe) vdWHs. The top and side views of (a) T1-graphene/GdI$_2$, (b) T2-graphene/GdI$_2$, (c) T3-graphene/GdI$_2$, (d) T1-germanene/GdI$_2$, (e) T2-germanene/GdI$_2$, (f) T3-germanene/GdI$_2$, (g) T1-SiGe/GdI$_2$, (h)T2-SiGe/GdI$_2$, and (i) T3-SiGe/GdI$_2$ vdWHs. The interlayer distances of these vdWHs are marked in their side views.

Table S1. The total energies and binding energies of *X*/GdI_2 (*X* = graphene, germanene, and SiGe) vdWHs with different stacking patterns.

vdWHs	Stacking Patterns	Total energy (eV)	Binding energy (eV/atom)
graphene/GdI_2	T1	−307.192	-0.954
	T2	−307.170	-0.948
	T3*	−307.192	-0.954
germanene/GdI_2	T1	−119.759	-0.937
	T2	−119.473	-0.865
	T3	−119.544	-0.883
SiGe/GdI_2	T1	−122.028	-0.932
	T2	−121.743	-0.860
	T3	−121.778	-0.869

* The optimized atomic alignment of T3-type graphene/GdI_2 is consistent with that of T1-type graphene/GdI_2, leading to identical total energy and binding energy for both types.

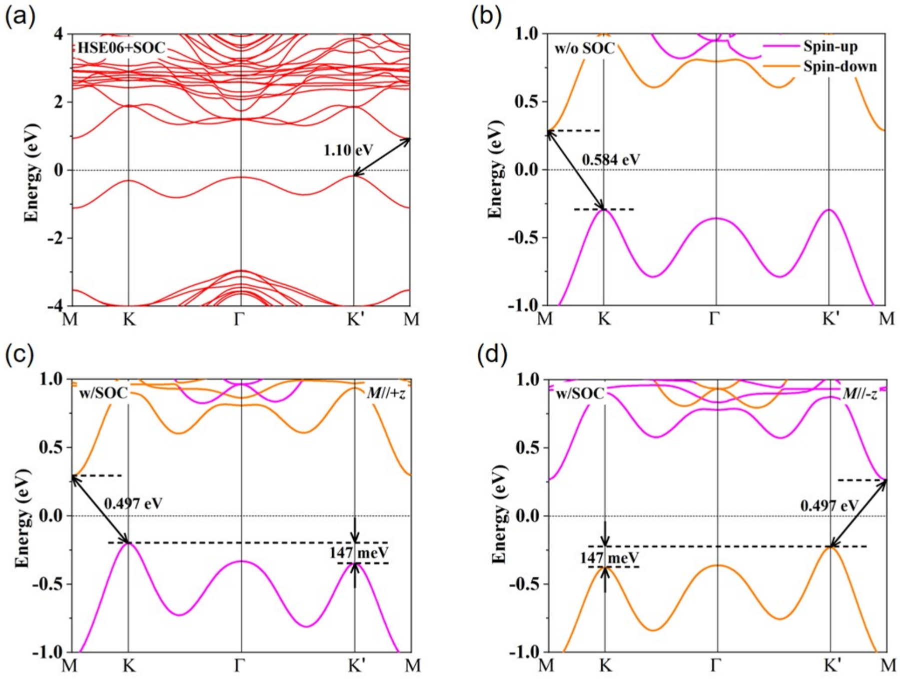

Fig. S3. Band structures of the isolated GdI_2 monolayer. Band structure of the GdI_2 monolayer calculated using (a) HSE06 with SOC and (b) PBE+U without SOC. Band structure of the GdI_2 monolayer with (c) positive and (d) negative magnetic moment along the *z*-direction in the presence of SOC, respectively. The pink and orange lines represent the spin-up and spin-down channels, respectively. The Fermi level is set to 0 eV.

As shown in **Fig. S3a,** the band gap value of the GdI_2 monolayer is 1.10 eV by the HSE06 method with SOC. In the absence of SOC, the band structure of the GdI_2 monolayer calculated by the PBE+U method, as shown in **Fig. S3b**, reveals that the top valence band and the bottom conduction band are contributed by the spin-up and spin-down channels, respectively, indicating that the GdI_2 monolayer belongs to bipolar magnetic semiconductor. When considering the SOC, as shown in **Fig. S3c**, it is obvious that the energy value at the K point in the top valence band is larger than that at the K' point, showing the spontaneous valley polarization due to the time reversal symmetry broken. The calculated valley splitting of the GdI_2 monolayer is 147 meV, which is in good agreement with previous report (149 meV)[1] and larger than that of GdF_2 (55 meV), $GdCl_2$ (38 meV), and $GdBr_2$ (82 meV)[2]. The SOC effect exerts a significantly stronger influence on the valence band of the monolayer GdI_2 compared to the conduction band, resulting in a transformation from an n-type indirect bandgap (0.584 eV) to a p-type indirect bandgap (0.497 eV) semiconductor. Furthermore, reversing the magnetization of Gd atoms from +*z* to –*z* direction, as shown in **Fig. S3d**, the top valence band and the bottom conduction band are transformed to be contributed by the spin-down and spin-up channels, respectively. Meanwhile, the energy at the K point in the top valence band is 147 meV lower than that at the K' point. The result indicates that reversing the magnetization direction has caused the inversion of both the spin and valley polarization of the GdI_2 monolayer .

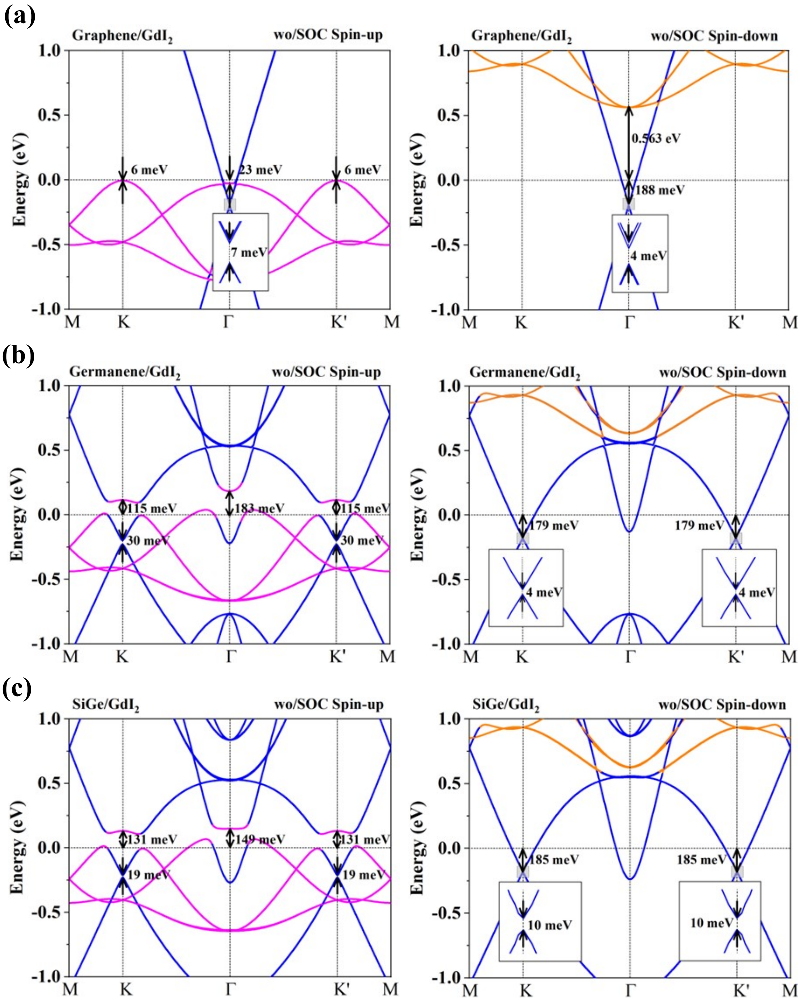

Fig. S4. Projected band structures of *X*/GdI$_2$ vdWHs. Projected band structures showing the spin-up and spin-down channels for (a) graphene/GdI$_2$, (b) germanene/GdI$_2$, and (c) SiGe/GdI$_2$ in the absence of SOC, respectively. The pink, orange and blue lines represent the contributions from the spin-up channel of GdI$_2$, the spin-down channel of GdI$_2$, and *X*, respectively. The illustrations provide enlarged views of the 2D Dirac cones and their corresponding band gaps. The Fermi level is set to 0 eV.

When SOC is not considered, the projected band structures with spin-up and spin-down channels of *X*/GdI$_2$ are shown in **Fig. S4a-c**. It is clear that the Dirac cones of 2D semimetals *X* shift downward relative to the Fermi level of the *X*/GdI$_2$ vdWHs. The direction of the Dirac cone shift in *X*/GdI$_2$ is opposite to that observed in RuCl$_2$/graphene and NbSe$_2$/graphene vdWHs[3], due to the opposite directions of charge transfer. Specifically, the Dirac point of Dirac semimetals *X* in graphene/GdI$_2$, germanene/GdI$_2$ and SiGe/GdI$_2$ deviate downward from the Fermi level by about 188 meV, 179 meV and 185 meV, respectively. More interestingly, the Dirac cones of the Dirac semimetals exhibit opened band gaps due to the effects of the vdW interaction between GdI$_2$ and Dirac semimetals *X*. The spin-up (spin-down) channel of GdI$_2$ induces band gaps of 7 meV (4 meV) in graphene, 30 meV (4 meV) in germanene, and 19 meV (10 meV) in SiGe, respectively. The spin-up channel of GdI$_2$ causes the Dirac semimetals to open a relatively larger bandgap, further demonstrating that the spin-up channel of GdI$_2$ has a greater effect on the electronic structure of the Dirac semimetals.

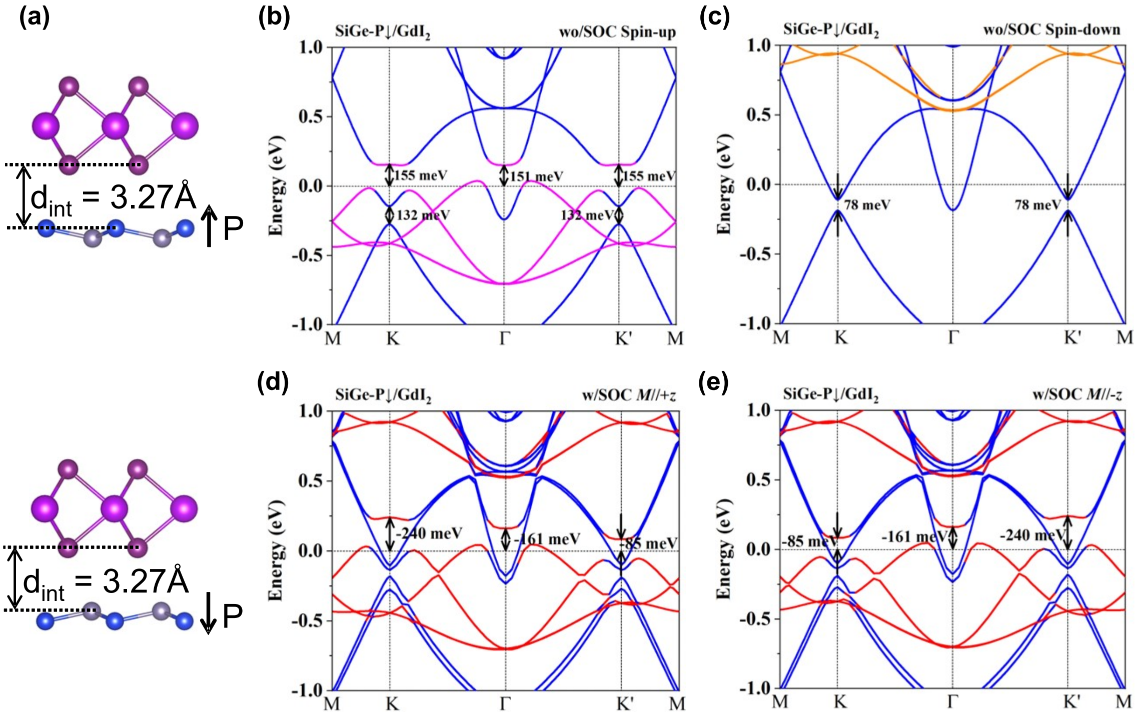

Fig. S5. Side views and projected band structures of SiGe/GdI$_2$ vdWH with different spontaneous polarization. (a) Side views of the SiGe/GdI$_2$ vdWH with SiGe polarized upward (P↑) and downward (P↓), respectively. Projected band structures of SiGe-P↓/GdI$_2$ vdWHs with (b) spin-up channel (pink lines) and (c) spin-down channel (orange lines) in the absence of SOC, respectively. Projected band structures of SiGe-P↓/GdI$_2$ vdWHs with (d) positive and (e) negative magnetic moment along the *z*-direction in the presence of SOC, respectively. The red and blue lines represent the contributions from GdI$_2$ and *X*, respectively. The Fermi level is set to 0 eV.

It is noteworthy that the SiGe monolayer is a 2D ferroelectric semimetal with out-of-plane spontaneous polarization[4]. The SiGe monolayer has also been employed in the design of ferroelectric field-effect transistors (FeFETs)[5-8]. Therefore, it is crucial to investigate the impact of ferroelectric polarization inversion in SiGe on the band structure and contact barrier of the SiGe/GdI$_2$ vdWH. The side views of SiGe/GdI$_2$ vdWH with SiGe polarized upward (P↑) and downward (P↓) are shown in **Fig. S5a**. When the ferroelectric polarization direction of SiGe is reversed from upward (P↑) to downward (P↓), as shown in **Fig. S5b,c**, the open band gap of Dirac points at the K point and K' points increases from 19 meV (10 meV) to 132 meV (78 meV) in the spin-up (spin-down) channel of GdI$_2$, respectively, meaning that the interlayer interactions are stronger when Ge atoms are close to GdI$_2$. When SOC is considered, SiGe/GdI$_2$ vdWH remains a p-type overall Ohmic contact with the p-type SBHs of −240 meV and −85 meV at the K and K' points, respectively, even as the polarization direction of SiGe reverses from upward to downward, as shown in **Fig. S5d,e**. It can be seen that the reversal of ferroelectric polarization in SiGe does not change the intrinsic contact type of the SiGe/GdI$_2$ vdWH. Therefore, unless otherwise specified, the polarization direction of SiGe is assumed to be upward in this work.

The equilibrium interlayer distances of graphene/GdI_2, germanene/GdI_2, and SiGe/GdI_2 vdWHs are 3.61 Å, 3.24 Å, and 3.27Å, respectively. The change of interlayer distance (Δd) is defined as:

$$\Delta d = d_{int} - d_0 \tag{1}$$

where d_{int} and d_0 refer to the changed and the equilibrium interlayer distances of *X*/GdI_2 vdWHs, respectively.

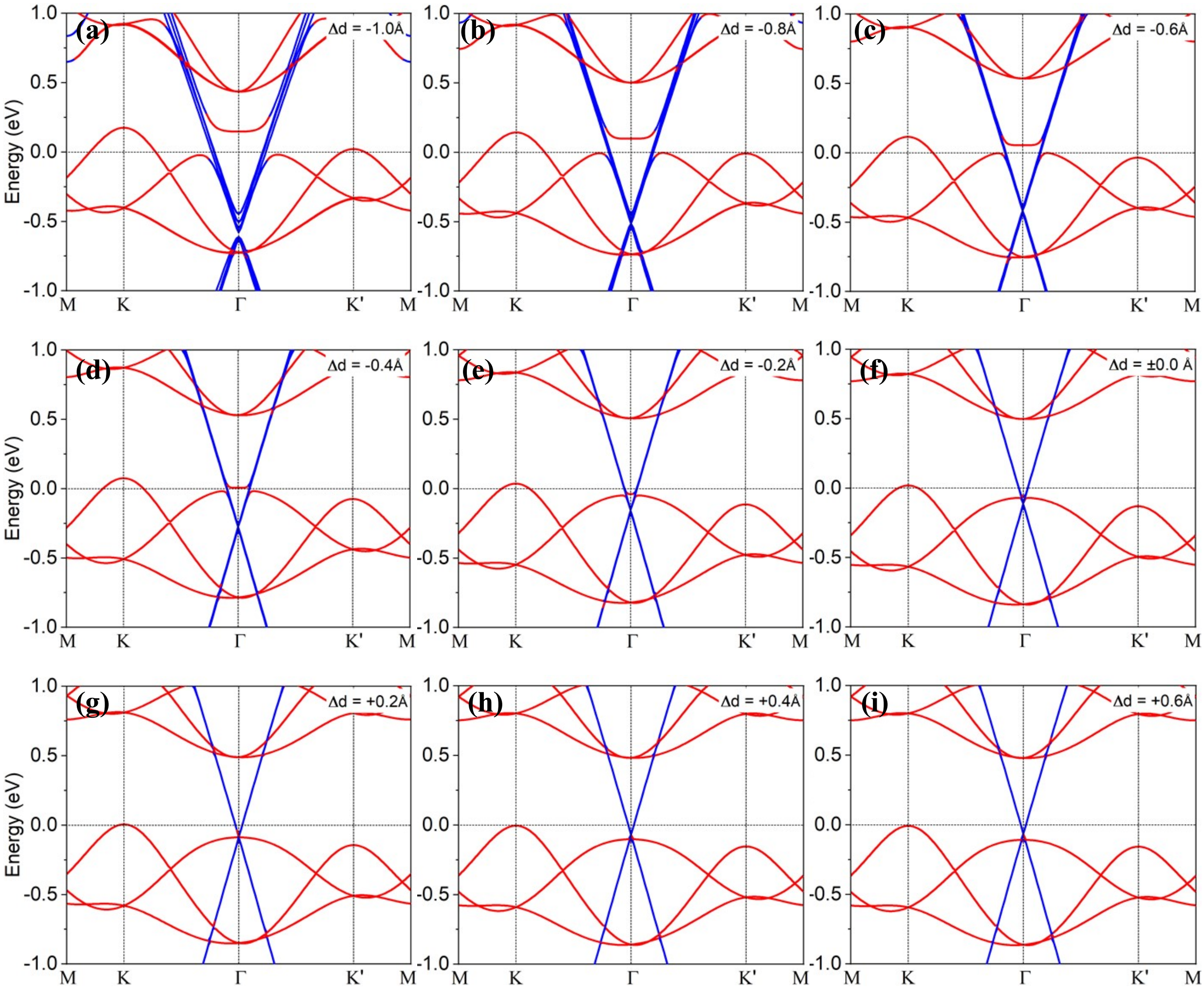

Fig. S6. Projected band structures of graphene/GdI_2 vdWH with SOC under different interlayer distances. The red and blue lines in the band structures represent the contributions from GdI_2 and graphene, respectively. The Fermi level is set to 0 eV. The fully relaxed interlayer distance of graphene/GdI_2 is 3.61 Å (Δd = ±0.0 Å).

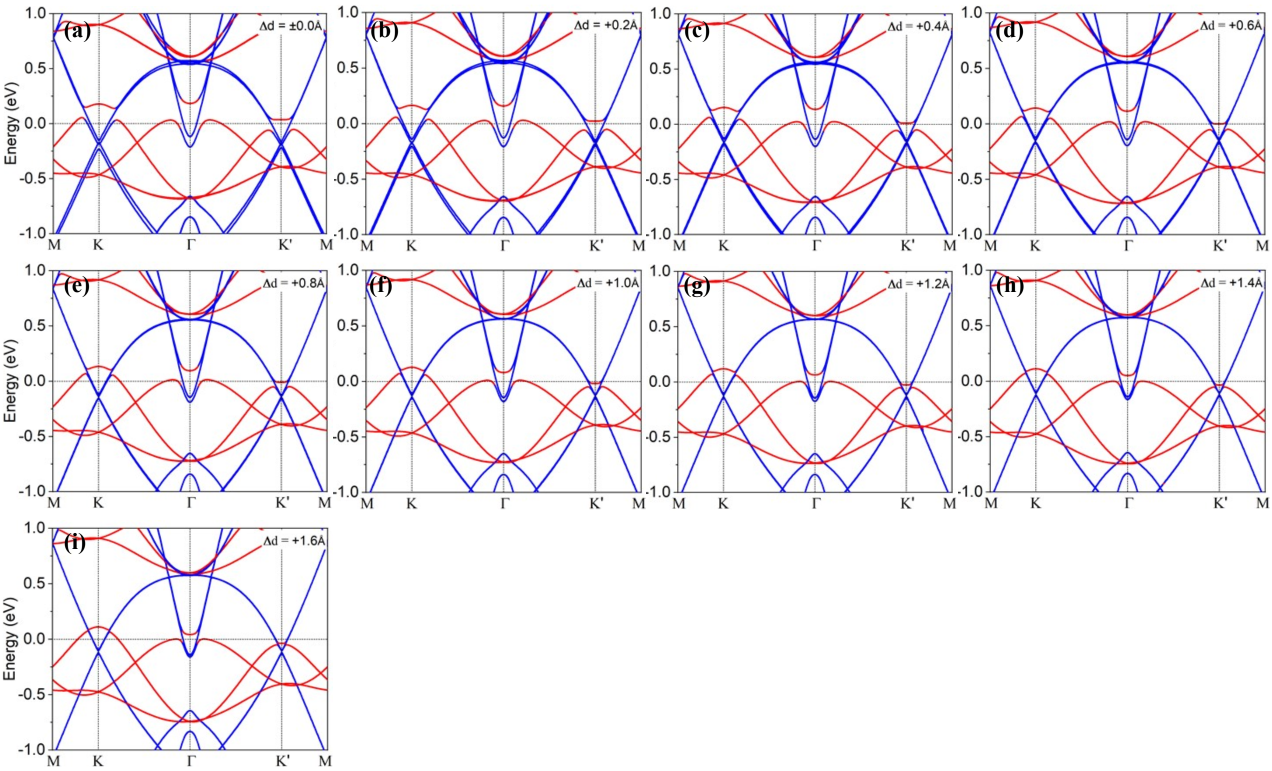

Fig. S7. Projected band structures of germanene/GdI$_2$ vdWH with SOC under different interlayer distances. The red and blue lines in the band structures represent the contributions from GdI$_2$ and germanene, respectively. The Fermi level is set to 0 eV. The fully relaxed interlayer distance of germanene/GdI$_2$ is 3.24 Å (Δd = ±0.0 Å).

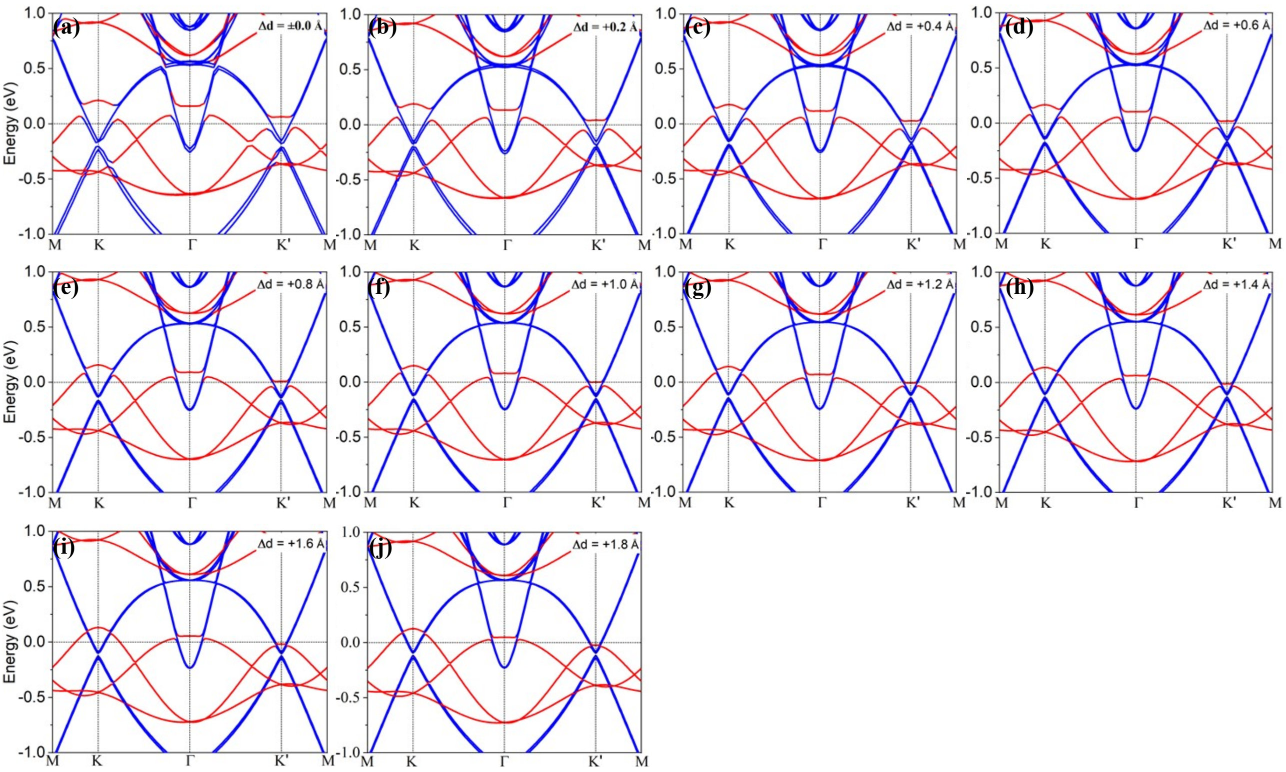

Fig. S8. Projected band structures of SiGe/GdI$_2$ vdWH with SOC under different interlayer distances. The red and blue lines in the band structures represent the contributions from GdI$_2$ and SiGe, respectively. The Fermi level is set to 0 eV. The fully relaxed interlayer distance of SiGe/GdI$_2$ is 3.27 Å (Δd = ±0.0 Å).

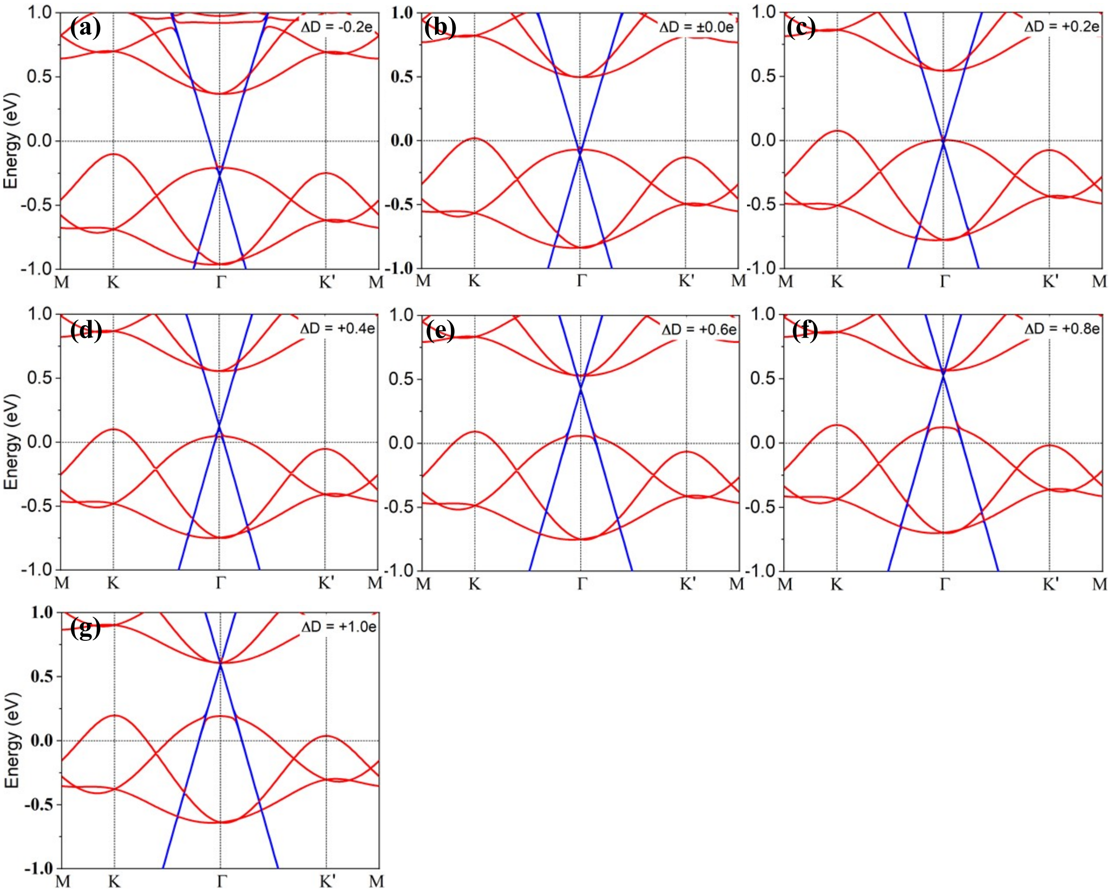

Fig. S9. Projected band structures of graphene/GdI$_2$ vdWH with electron and hole doping from -0.2 e to +1.0 e. Positive and negative values indicate electron and hole doping, respectively. The red and blue lines in the band structures represent the contributions from GdI$_2$ and graphene, respectively. The Fermi level is set to 0 eV.

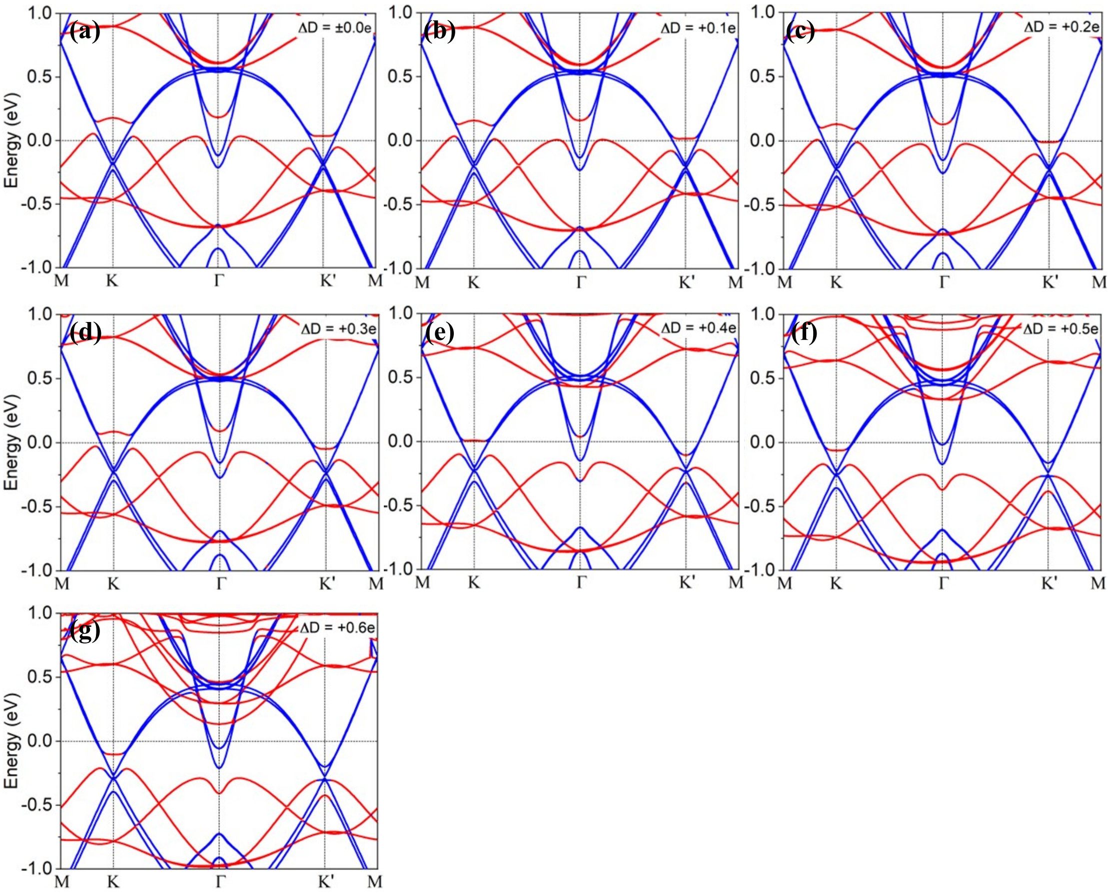

Fig. S10. Projected band structures of germanene/GdI$_2$ vdWH with electron doping from 0 e to 0.6 e. The red and blue lines in the band structures represent the contributions from GdI$_2$ and germanene, respectively. The Fermi level is set to 0 eV.

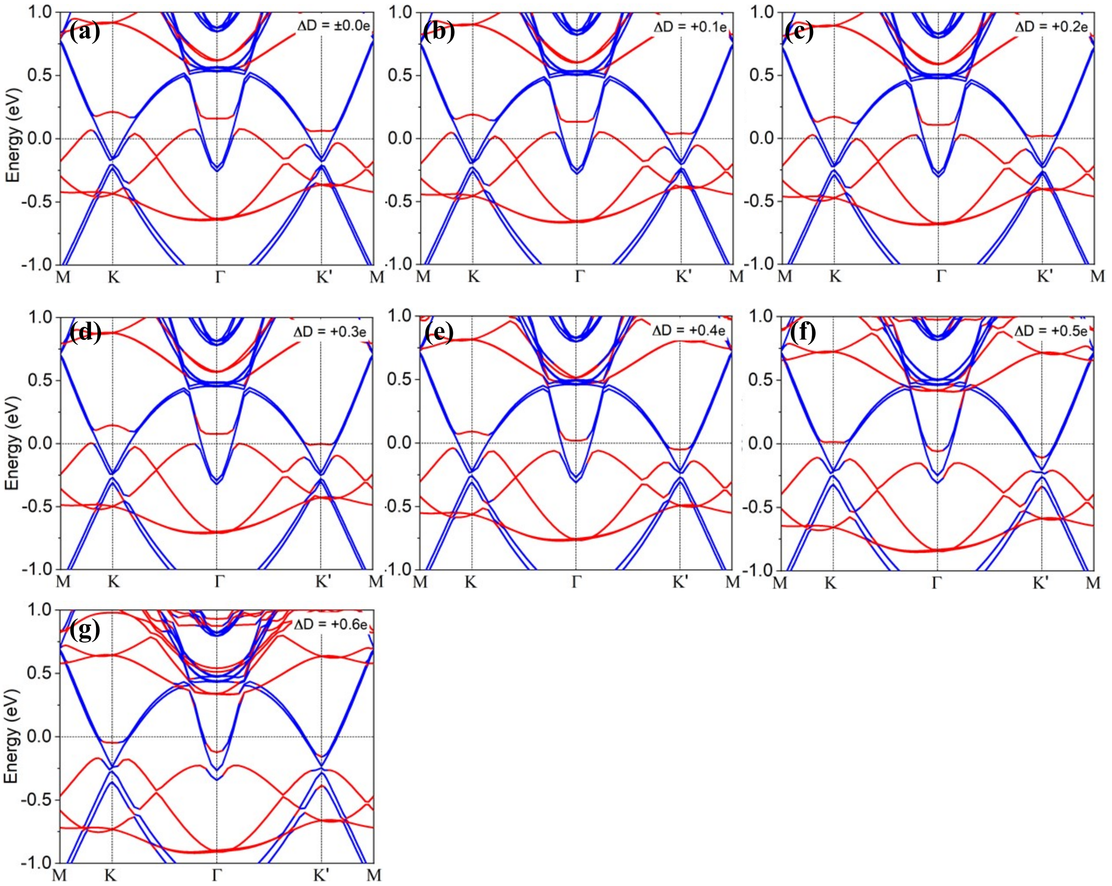

Fig. S11. Projected band structures of SiGe/GdI$_2$ vdWH with electron doping from 0 e to 0.6 e. The red and blue lines in the band structures represent the contributions from GdI$_2$ and SiGe, respectively. The Fermi level is set to 0 eV.

References

1 H.-X. Cheng, J. Zhou, W. Ji, et al., *Physical Review B*, 2021, **103**, 125121.

2 K. Sheng, H. K. Yuan and Z. Y. Wang, *Physical Chemistry Chemical Physics*, 2022, **24**, 3865-3874.

3 X. Feng, C. S. Lau, S. J. Liang, et al., *Advanced Functional Materials*, 2023, **34**, 2309848.

4 C. J. Yao, H. F. Huang, Y. Yao, et al., *Journal of Physics: Condensed Matter*, 2021, **33**, 145302.

5 A. Vinod, P. Kumar and B. Bhowmick, *AEU - International Journal of Electronics and Communications*, 2019, **107**, 257-263.

6 M. Lederer, F. Muller, K. Kuhnel, et al., *IEEE Electron Device Letters*, 2020, **41**, 1762-1765.

7 N. Thoti and Y. Li, *Japanese Journal of Applied Physics*, 2021, **60**, 054001.

8 S. Singh, R. Gupta, Priyanka, et al., *Silicon*, 2022, **14**, 11015-11025.